The Astrophysical Journal, 812:79 (9pp), 2015 October 10 doi:10.1088/0004-637X/812/1/79

THE EXTREME ULTRAVIOLET DEFICIT: JET CONNECTION IN THE QUASAR 1442+101

Brian Punsly[1,2], Paola Marziani[3], Preeti Kharb[4], Christopher P. O'Dea[5,6], and Marianne Vestergaard[7]
[1] 1415 Granvia Altamira, Palos Verdes Estates CA 90274, USA; brian.punsly1@verizon.net
[2] ICRANet, Piazza della Repubblica 10 Pescara, I-65100, Italy
[3] INAF, Osservatorio Astronomico di Padova, Italia
[4] Indian Institute of Astrophysics, II Block, Koramangala, Bangalore 560034, India
[5] Department of Physics and Astronomy, University of Manitoba, Winnipeg, MB R3T 2N2, Canada
[6] School of Physics & Astronomy, Rochester Institute of Technology, Rochester, NY 14623, USA
[7] Dark Cosmology Centre, Niels Bohr Institute, University of Copenhagen, Juliane Maries Vej 30, DK-2100 Copenhagen ϕ, Denmark
Received 2015 August 8; accepted 2015 September 8; published 2015 October 9

ABSTRACT

In previous studies, it has been shown that the long-term time-averaged jet power, $\overline{Q}$, is correlated with spectral index in the extreme ultraviolet (EUV), $\alpha_{\rm EUV}$ (defined by $F_\nu \sim \nu^{-\alpha_{\rm EUV}}$ computed between 700 and 1100 Å). Larger $\overline{Q}$ tends to decrease the EUV emission. This is a curious relationship because it connects a long-term average over $\sim 10^6$ years with an instantaneous measurement of the EUV. The EUV appears to emit adjacent to the central supermassive black hole and the most straightforward explanation of this correlation is that the EUV-emitting region interacts in real time with the jet-launching mechanism. Alternatively stated, the $\overline{Q}$–$\alpha_{\rm EUV}$ correlation is a manifestation of a contemporaneous (real time) jet power, $Q(t)$, correlation with $\alpha_{\rm EUV}$. In order to explore this possibility, this paper considers the time variability of the strong radio jet of quasar 1442+101, which is not aberrated by strong Doppler enhancement. This high-redshift ($z = 3.55$) quasar is uniquely suited for this endeavor as the EUV is redshifted into the optical observing window allowing for convenient monitoring. More importantly, it is bright enough to be seen through the Lyman forest and its radio flux is strong enough that it has been monitored frequently. Quasi-simultaneous monitoring (five epochs spanning $\sim$40 years) shows that increases in $Q(t)$ correspond to decreases in the EUV as expected.

Key words: accretion, accretion disks – black hole physics – galaxies: active – galaxies: jets – magnetohydrodynamics (MHD)

1. INTRODUCTION

Powerful relativistic radio jets have been associated with the most intrinsically luminous ultraviolet emitters in the universe, namely quasars, since their discovery over 50 years ago. Only a small fraction of all quasars ($\sim$10%) have strong jets (radio loud quasars RLQs), and even fewer have radio lobes on supergalactic scales; $\sim$1.7% of all quasars have such extended structure (deVries et al. 2006). However, until recently there have been no observations of the jet-launching region, so there has been much speculation as to the mechanism that creates these jets. The literature is filled with numerical models and theories (Lovelace 1976; Blandford & Znajek 1977; Blandford & Payne 1982; Punsly 2008). There is no discriminant for authenticity due to a lack of direct measurement of the jet-launching region. However, this has changed recently with the examination of extreme ultraviolet (EUV) spectra shortward of the peak of the spectral energy distribution (SED) at 1100 Å. The quasar luminosity is widely believed to arise from the viscous dissipation of turbulence driven by the differential rotational shearing of accreting gas (Lynden-Bell & Rees 1971; Shakura & Sunyaev 1973). In numerical and theoretical models, the highest frequency optically thick thermal emission arises from the innermost region of the accretion flow and its frequency is shortward of the peak of the SED (Zhu et al. 2012). The EUV spectrum beyond the peak of the SED of quasars is the putative Wien tail of the emission of the innermost thermal component of the accretion flow which is adjacent to the central black hole (Marshall 1997; Punsly 2014). If $\overline{Q}$ is the long-term ($\sim 10^6$ years) time-averaged jet power (as determined from radio lobe emission and morphology) and $L_{\rm bol}$ is the bolometric thermal emission associated with the accretion flow, it was shown in Punsly (2014, 2015b) that jet efficiency, $\overline{Q}/L_{\rm bol}$, (which depends on a long-term average) was correlated with the deficit of EUV emission in RLQs relative to radio quiet quasars (RQQs) quantified by $\alpha_{\rm EUV}$ (the flux density scales as $F_\nu \propto \nu^{-\alpha_{\rm EUV}}$ and is computed between 1100 and 700 Å). This is the fundamental correlation and a partial correlation analysis shows that the correlation that exists between $\overline{Q}$ and $\alpha_{\rm EUV}$ is spurious (Punsly 2015b). This provides the first connection between jet power and an observable from a region that is likely contiguous or coincident with the jet-launching region in quasars.

This is a curious circumstance since the plasma in the radio lobes that is used to determine $\overline{Q}$ was ejected from the central engine $\sim 10^6$ years before the EUV-emitting gas reached the environs of the central black hole. Two parameters, $L_{\rm bol}$ and $\alpha_{\rm EUV,}$ are "real time" diagnostics of the quasar at the time of observation and $\overline{Q}$ is a long-term time average. Why should these parameters be connected in what is likely a time-variable system? It was concluded based on a statistical argument that the most logical explanation is that there is an underlying real time connection between the instantaneous jet power, $Q(t)$, and $\alpha_{\rm EUV}$ (Punsly & Marziani 2015). It is too much of a coincidence that two highly dynamic elements emanating from a common region are strongly correlated if there is no real time connection. The scatter seen in the correlation (see Figure 1) includes the variation of $L_{\rm bol}$ and $\alpha_{\rm EUV}$ from their long-term time-averaged value and the degree of scatter indicates that in general these variations are modest.

In this paper, a search is initiated for the real time connection between $Q(t)/L_{\rm bol}$ and $\alpha_{\rm EUV}$. This is a daunting task since it is not trivial to find an estimator that scales with $Q(t)$ that is

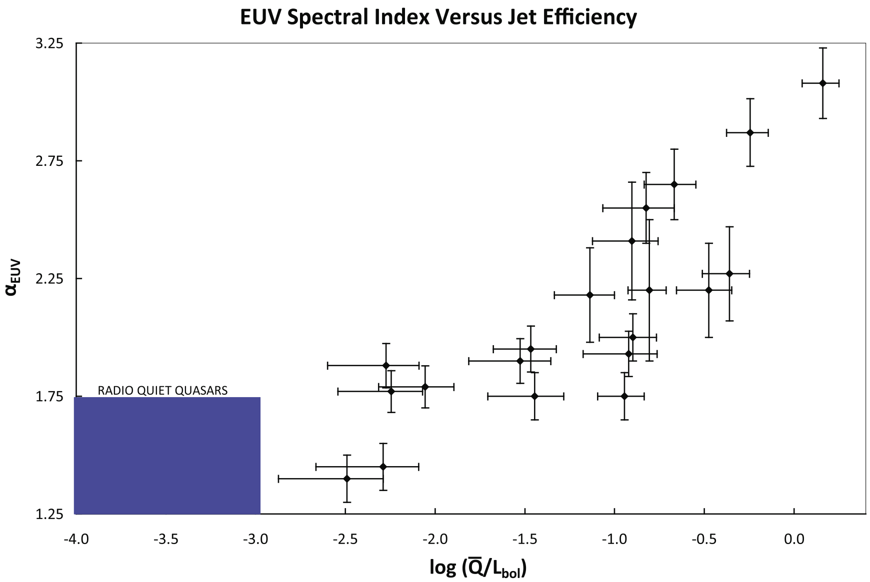

Figure 1. Correlation of $\alpha_{\rm EUV}$ vs. jet efficiency, $\overline{Q}/L_{\rm bol}$ (Punsly 2015b; Punsly & Marziani 2015). More powerful jets have depressed EUV emission.

reliable and there is simply not enough observing time on the *Hubble Space Telescope* (*HST*) to monitor quasar continua (spectra are needed to excise the emission lines) in the EUV. Sufficient monitoring requires observing a source with Earth-based telescopes which requires $z > 3$ in order to view the EUV redshifted into the U or B bands. This is not ideal due to the large flux attenuation by the intervening Lyα forest. First, the quasar must have an incredibly large intrinsic EUV luminosity in order to shine brightly enough to be seen easily through the absorbing screen. The second requirement is that the radio luminosity should be high enough so that the object appears frequently in survey work so that there is an ample database to cull through for quasi-simultaneous observations. The third requirement is almost mutually exclusive from the first two. In order to monitor $Q(t)$ by radio flux, the source cannot suffer from Doppler aberration. This is necessary since small variations in geometry would appear as significant changes in the observed flux and this would provide a false indicator of changes in the intrinsic jet luminosity (Lind & Blandford 1985). Most of the radio sources at $z > 3$ in the older radio catalogs have sufficient flux density because they are Doppler enhanced. Thus, we have a very strong set of restrictions due to the high redshift, luminosity, and lack of Doppler beaming: the source needs an enormous intrinsic radio luminosity with no significant Doppler beaming (i.e., $\sim$1 Jy at $z > 3$ with no Doppler beaming). Do such sources exist? They seem to in the form of gigahertz peak radio sources (GPS). Some of these at high redshift are incredibly luminous (O'Dea 1998). We argue below that the quasar 1442+101 at $z = 3.55$ is a suitable candidate.

2. SOURCE SELECTION

The high redshift quasar, 1442+101, is a powerful radio source that appeared in many of the early radio surveys. The spectrum peaks at ≈1 GHz at 2.5 Jy. Therefore, it was very surprising that the source was at extremely high redshift. It was also surprising that, unlike other high redshift sources that appear in radio surveys, it is not blazarlike in that it is not highly variable at radio frequencies.

2.1. Doppler Beaming

It is argued here that the radio emission at frequencies below 10 GHz is not Doppler beamed in 1442+101. A list of evidence of Doppler beaming occurs below. For each item in the list, the actual circumstance observed in 1442+101 is listed after the colon.

1. Extreme radio variability: not evident in the large data set compiled in the NASA Extragalactic Database or monitoring in Tingay et al. (2003) and Mingaliev et al. (2012). This is indicative of non-blazar radio emission.
2. Superluminal motion on 30–100 pc scales: there is no measurable change in position of the three components seen at 1.6 GHz very long baseline interferometry (VLBI) images in 1989 and in the 2.3 GHz VLBI images from 1999 on scales of 10–100 pc (Dallacasa et al. 1995; Pushkarev & Kovalev 2012). No blazarlike parsec-scale evolution has been observed.
3. Flat spectrum radio core to >30 GHz in the quasar rest frame: the spectrum is very steep with a spectral index $\alpha > 1$ above 30 GHz in the quasar rest frame (Kovalev et al. 2004; Mantovani et al. 2009). The spectrum continues to steepen toward 1000 GHz in the quasar rest frame (Steppe et al. 1995). Thus, there is no "buried" flat spectrum core embedded within the source of the gigahertz peaked emission. There is insignificant blazar-like synchrotron self-absorption at high frequency.
4. Large optical variability: low optical variability is reported (Pica et al. 1988; Smith et al. 1993). The optical variability is similar to that of RQQs and thus not typical of blazars.
5. Large optical polarization: no measurements exist. There is inconclusive evidence of blazar activity.

The preponderance of evidence indicates that Doppler beaming does not affect the emission from 1442+101 significantly.

2.2. Estimator for $Q(t)$

If a source is not Doppler beamed then it seems reasonable to choose the optically thin radio luminosity created in the most

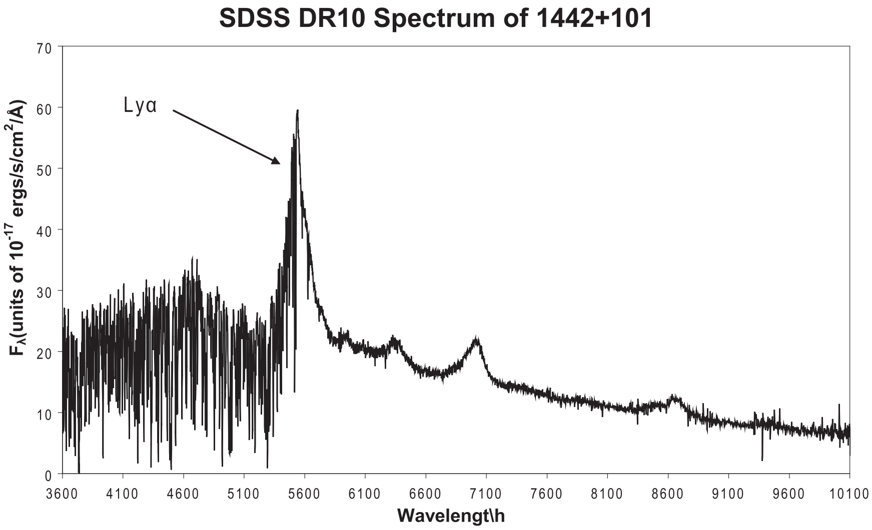

Figure 2. Note the ample flux shortward of Lyα in the SDSS DR 10 spectrum of 1442+101.

compact regions of the source as a quantity that scales with jet power. This emanates inside of any working surface (a region of intense jet dissipation such as an interaction with a dense cloud) and without synchrotron self-absorption we are looking directly at the synchrotron emission that directly reflects dynamical elements, the energy of electrons, and the energy of the magnetic field in the jet. It might not be a linear relationship, but increases in the optically thin radio emission from the innermost jet should be positively correlated with the jet power. The quasar 1442+101 is one of the most compact radio sources known (van Breugel et al. 1984). There is no emission, even in deep observations, on kiloparsec scales (Murphy et al. 1993). Based on VLBI images of GPS quasars at lower redshift (higher spatial resolution than is possible with 1442+101 observations), the radio emission is highly resolved with a small fraction in the core, unlike the case of blazars (Stanghellini et al. 1997, 2001). Most of the emission, especially at lower frequencies, comes from knots in the jet >10 pc from the core, the putative working surface. This is the primary source of the optically thick low frequency emission in most GPS quasars and likely 1442+101 as well. To estimate $Q(t)$, it is not appropriate to sample the optically thick radio emission from the "working surface" which depends on dissipation that is determined by dynamics and physical conditions external to the jet. Above 8.4 GHz (observer frame) the spectral index is $\alpha > 1$ (optically thin) and this frequency is sampled frequently (Kovalev et al. 2004; Mantovani et al. 2009; Mingaliev et al. 2012). Thus, the 8.4 GHz flux density should be an indicator of jet strength well inside the working surface. VLBI imaging at 8.6 GHz indicates that the majority of the 8.4 GHz flux is unresolved inside of 50 light years from the source (Pushkarev & Kovalev 2012). This is the surrogate for monitoring jet power, given the insufficient monitoring at higher frequencies.

2.3. EUV Penetration of the Lyman Forest

The most startling aspect of 1442+101 is that the EUV emission is so bright that it shines through a dense forest of Lyα absorbing clouds. The spectrum in Figure 2 indicates that there is more than adequate luminosity to sample the spectrum at $\lambda_o = 4000$ Å (observer frame) corresponding to $\lambda_e = 880$ Å in the quasar rest frame. The flux measured is not the intrinsically emitted flux, but that attenuated by the Lyman forest. About five or six absorbers have been resolved spectroscopically in a $\delta\lambda_o = 100$ Å window centered at $\lambda_o = 4000$ Å (Baldwin et al. 1974; Barthel et al. 1990). The intervening gas is composed of many small absorbing clouds, so one does not expect significant time variation in the total flux integrated over a 100 Å window due to changes in the total absorbing column. By measuring the EUV continuum at $\lambda_e = 880 \pm 11$ Å we avoid contamination by emission lines (Telfer et al. 2002). The 100 Å "smoothing" window minimizes any effects caused by spectral resolution differences between observations and the narrow absorption lines, allowing for a consistent method of determining the observed flux density at $\lambda_o = 4000$ Å.

3. RESULTS

There are far more radio observations than calibrated optical spectra down to $\lambda_o = 4000$ Å. The optical and radio variability is small (Pica et al. 1988; Tingay et al. 2003). Due to the paucity of optical data sampling it thus seems reasonable (but not ideal) to consider observations within 300 days as quasi-simultaneous. Due to cosmological redshifting, this corresponds to about 66 days in the quasar rest frame. To put this in perspective, we estimate the size of the putative active EUV/radio-emitting region in 1442+101 as follows. Based on standard bolometric corrections, Figure 2, and archival IR (rest frame optical) data from the NASA Extragalactic Database, we estimate $L_{\rm bol} \approx 4\text{–}5 \times 10^{47}$ erg s^{-1}, ignoring the contribution from reprocessed emission (avoiding double counting) in the molecular clouds (Davis & Laor 2011; Punsly 2015b). If the accretion flow is radiating at <50% of the Eddington rate, the black hole mass would be $M_{\rm bh} > 8 \times 10^9\, M_\odot$. For a rapidly spinning black hole, 66 days corresponds to <2 Keplerian orbital periods at a distance of $5R_g$ ($R_g > 1.1 \times 10^{15}$ cm is the black hole radius for a rapidly rotating black hole) from the central black hole in the equatorial plane. This also corresponds to <4 Keplerian orbital periods at a distance of $3R_g$ from the central black hole in the equatorial plane. These are reasonable estimates for the location of the EUV-emitting region from the variability of the EUV and numerical models of accretion flows

Table 1
Quasi-simultaneous EUV and Radio Variability of 1442+101

Observation Date (MJD) Radio/Optical	Flux Density 8.46 GHz (mJy)	Flux Density $\lambda_o = 4000$ Å ($\lambda_e = 880$ Å) (10^{-17} erg s^{-1} cm^{-2} Å^{-1})	Telescope Radio/Optical	Delta[a] (Days)
42126/42189	598 ± 42[b]	23.4 ± 2.4[c]	Parkes 64 m/Lick 3 m	297
47266/47320	709 ± 18[d]	15.3 ± 2.3[e]	VLA/Hale 5 m	54
48415/48427	704 ± 18[d]	16.4 ± 1.2[f]	VLA/Lick 3 m	12
53940/53827	663 ± 16[d]	21.3 ± 1.3[d]	VLA/SDSS DR7	113
55834/55976	659 ± 16[d]	20.5 ± 1.4[d]	VLA/SDSS DR10	142

Notes.
[a] Number of days between radio and optical observations.
[b] Shimmins & Bolton (1981).
[c] Baldwin et al. (1974).
[d] This paper.
[e] Barthel et al. (1990).
[f] Lyons et al. (1995).

(Marshall 1997; Haba et al. 2003; Zhu et al. 2012; Punsly 2014, 2015b). Thus, 300 days is not that unreasonable of a condition for quasi-simultaneity in the context of jet production and EUV emission.

Table 1 shows the data for the five quasi-simultaneous epochs that are spread out over ~40 years (1973–2012). Table 1 lists the date of observations (column 1), the 8.46 GHz flux density (column 2), the flux density at $\lambda_o = 4000$ Å (column 3), the telescopes (column 4), the difference in the observation date between the optical and radio in days (column 5). For observations that are at a slightly different frequency than 8.46 GHz (~100–400 MHz), a spectral index of 1 is assumed based on the MJD 47266 VLA observations at 8.21 and 8.66 GHz and archival data (Mantovani et al. 2009; Kovalev et al. 2004; Mingaliev et al. 2012). We note that the observation in Barthel et al. (1990) on MJD 47320 in Table 1 is chosen to have the largest fractional uncertainty, 15%, of all the epochs. Issues with the flux calibration have been noted based on the atmospheric dispersion correction for the Barthel et al. (1990) sample (Corbin 1991). For SDSS DR10 quasar data, such as the MJD 55976 observation in Table 1, there is a calibration issue in the blue part of the spectrum. Specifically, in order to increase spectral sensitivity for quasars, the hole drilled over the aperture is centered on the displacement associated with 4000 Å. However, the calibration of the star has a hole centered about the displacement associated with 5400 Å. This inconsistency artificially raises the flux level in the blue which we estimate as a 7.2% excess for quasar light at 4000 Å (from the airmass of 1.1 and seeing of 1.4 arcsec). If there is a similar underestimate of the standard star flux at 4000 Å, the total estimated increase in the DR10 quasar spectral flux is 14.4% at 4000 Å. As a check of this calculation, we note that this agrees with the offset seen between the photometric g magnitude and the synthetic magnitude computed from the spectrum (18.61 and 18.39, respectively). The corrected spectrum is plotted in Figure 2.

Table 1 can be used to assess the real time connection between $Q(t)/L_{\text{bol}}$ and α_{EUV}. Note that, per the discussions by Punsly (2015b), $L_{\text{bol}} \approx 3.8F_{\lambda_e}(\lambda_e = 1100\text{ Å})$ in the quasar rest frame and $\alpha_{\text{EUV}} = \log \frac{F_{\lambda_e}(\lambda_e = 880\text{ Å})}{F_{\lambda_e}(\lambda_e = 1100\text{ Å})} \Big/ \log \frac{880\text{ Å}}{1100\text{ Å}}$.[8] Thus, α_{EUV} varies monotonically with $F_{\lambda_e}(\lambda_e = 880\text{ Å})/F_{\lambda_e}(\lambda_e = 1100\text{ Å})$. If there is a relationship between $Q(t)/L_{\text{bol}}$ and α_{EUV} then there is a relationship between $Q(t)/L_{\text{bol}}$ and $F_{\lambda_e}(\lambda_e = 880\text{ Å})/F_{\lambda_e}(\lambda_e = 1100\text{ Å})$. The advantage of the latter relationship is that both quantities have $F_{\lambda_e}(\lambda_e = 1100\text{ Å})$ in the denominator. Thus if one multiplies both quantities by $F_{\lambda_e}(\lambda_e = 1100\text{ Å})$, one only needs to look at the light curves of $Q(t)$ (as traced by the 8.46 GHz flux density) and $F_{\lambda_o}(\lambda_o = 4000\text{ Å})$ (equivalently $F_{\lambda_e}(\lambda_e = 880\text{ Å})$) in order to detect a correlation between $Q(t)/L_{\text{bol}}$ and α_{EUV}. The motivation for this re-normalization is to remove the undesirable statistical scatter caused by dividing both the quantities by $F_{\lambda_o}(\lambda_o = 5000\text{ Å})$ (corresponding to $\lambda_e = 1100$ Å) which adds considerable uncertainty to each measured quantity, but does not add physical content. Such an expedience would not be justified in an analysis that comprised multiple objects since each object is normalized differently and the normalization is time variable.

The top frame of Figure 3 is a plot of both 8.46 GHz flux density and $F_{\lambda_o}(\lambda_o = 4000\text{ Å})$ as a function of time. The bottom frame of Figure 3 shows that $Q(t)$ decreases as $F_{\lambda_o}(\lambda_o = 4000\text{ Å})$ increases as expected. Even though the number of observations is too small for rigorous statistical analysis, we note that the Pearson correlation coefficient is −0.949, corresponding to a one-sided 99.3% statistical significance. If one restricts the analysis to a "gold sample" of epochs, all observed with the same telescope (the VLA) and within 150 days of the optical observation (<2 Keplerian orbits $3R_g$ from the black hole), one still sees a correlation. The two stronger radio states have the weakest $F_{\lambda_o}(\lambda_o = 4000\text{ Å})$ and vice versa for the two weaker radio states.

In the analysis of *HST* composite spectra in Punsly (2014) and Telfer et al. (2002), a deficit of EUV continuum emission was associated with the radio loudness in quasars. There was no deficit of emission seen in the far-UV continuum for RLQs. However, the continua plotted in Figure 4 indicate a far-UV

[8] Our spectra do not extend all the way to $\lambda_e = 700$ Å. A power law fits the continuum well in this range for other quasars (Punsly 2015b). Using $\lambda_e = 880$ Å to compute the power law should be an adequate expedience to see changes in spectral slope.

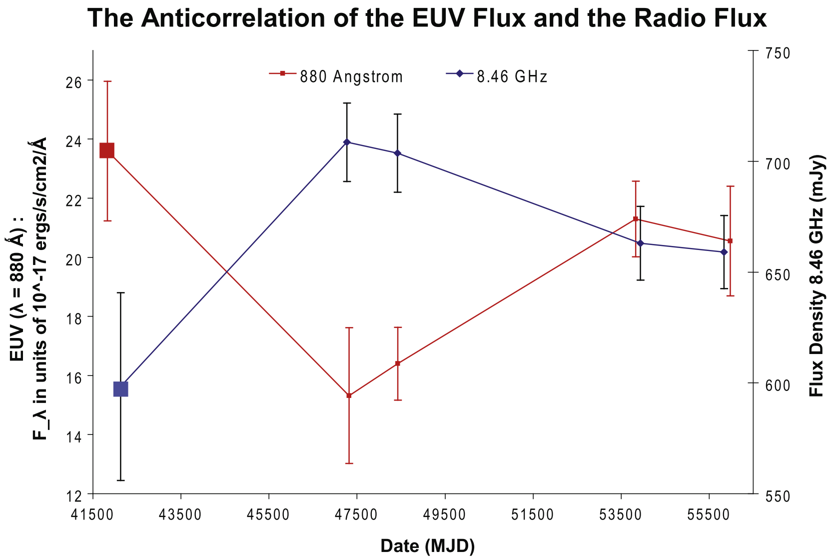

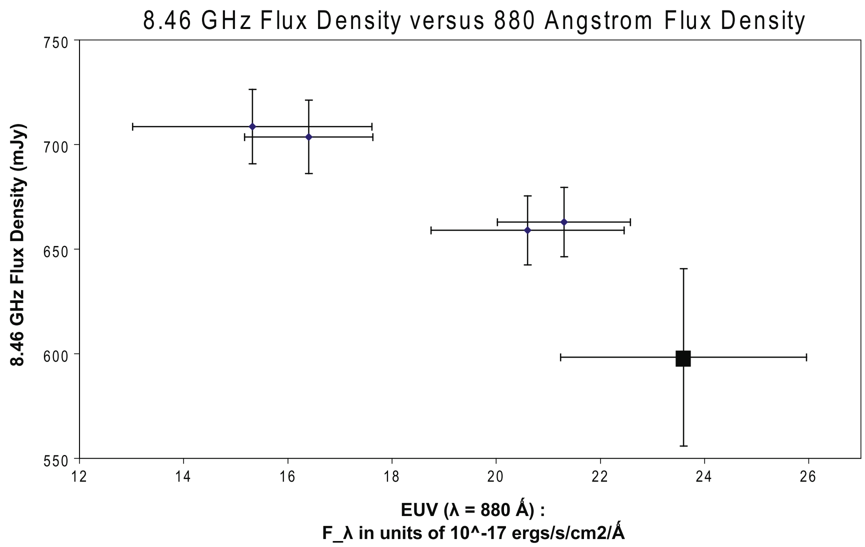

Figure 3. Top frame shows the light curves for EUV flux density and 8.46 GHz flux density sampled at quasi-simultaneous observation epochs. The bottom frame shows the anti-correlation of the EUV flux density and the 8.46 GHz flux density. The squares indicate the observational epoch that is not in the "gold sample" (not a VLA radio observation) described in the text.

continuum suppression as the jet gets stronger. The plot shows piecewise continuum spectra estimates in the far-UV and EUV at different epochs labeled by their 8.46 GHz flux density. The rest frame points were sampled at wavelengths in which line emission seemed minimal in all the spectra. Rest frame wavelengths were indicated for ease of comparison to well known emission lines. The observed wavelengths are 4000, 5000, 6200, 6700, and 7500 Å. There are three radio "weaker" jet states at 598, 659, and 663 mJy and two "stronger" jet states at 704 and 709 mJy. The UV fluxes are highly clustered at $\lambda_e = 1650$ Å, and four of the flux density measurements are not statistically significantly different. The flux density of the continua associated with the weak jet states exceeds that of the continua associated with the strong jet states by an ever increasing differential as the wavelength decreases. Furthermore, the EUV spectra from 1100 to 880 Å are softer (larger α_{EUV}) for the stronger jet states than for the weaker jet states as expected from a $Q(t)/L_{\mathrm{bol}}$ and α_{EUV} correlation. The continuum suppression associated with jet power might taper off in the far-UV as opposed to an abrupt turn off at $\lambda_e = 1100$ Å.

4. DISCUSSION

The physical interpretation of the correlation between jet power and the decrement in EUV luminosity that is illustrated in Figures 1, 3, and 4 was elucidated in two previous studies (Punsly 2014, 2015b). In this section, we review this analysis and discussion in order to put the results into perspective. The most straightforward explanation of the correlation involves jets from magnetic flux in the inner accretion disk where the EUV emission also originates. As more poloidal vertical magnetic flux is stored in the innermost accretion disk, the volume available for the thermal emitting gas is displaced. More poloidal magnetic flux equates to a stronger jet and less optically thick thermal gas equates to a weaker EUV luminosity. This dynamical configuration is known as magnetically arrested accretion (Igumenshchev 2008).

Many different dynamical systems have been classified as magnetically arrested in the numerical simulation literature. The relevant numerical simulations for RLQs are the ones in which the vertical magnetic flux is distributed in magnetic islands of low plasma density that are concentrated in the inner

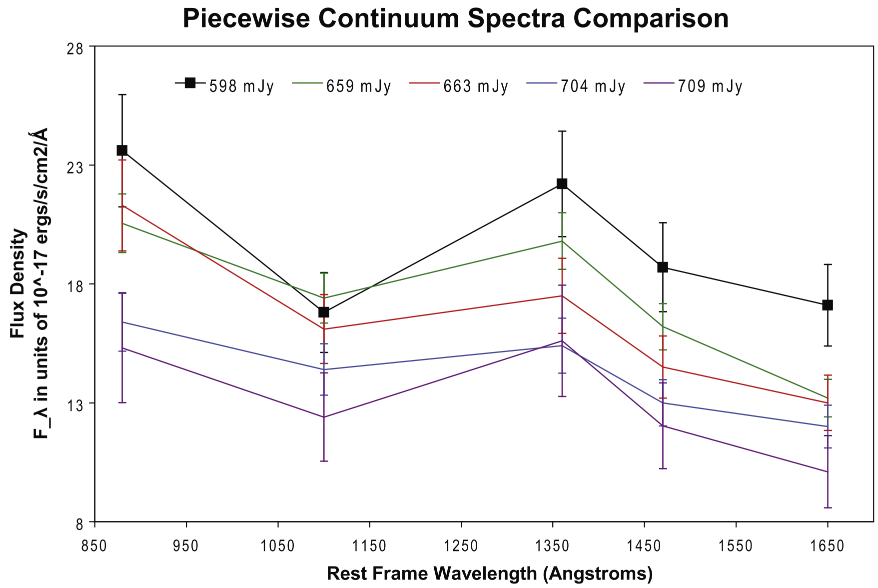

Figure 4. Piecewise continuum estimates in the far-UV and EUV of the different epochs labeled by their 8.46 GHz flux density. The squares indicate the observational epoch that is not in the "gold sample" (not a VLA radio observation) described in the text. The continuum excess of weak jet states relative to strong jet states is largest in the EUV.

accretion flow. The configuration is far from time stationary. The islands are dynamic and buoyantly move through the ram pressure imposed by the dense thermal EUV-emitting plasma by means of a series of Kruskal–Schwarzschild instabilities (Igumenshchev 2008). The ram pressure of the accretion flow concentrates magnetic flux near the black hole.

4.1. A Review of Evidence for Magnetically Arrested Accretion in RLQs

Evidence of the detailed predictions of magnetically arrested accretion was found in Punsly (2015b) by exploring a basic model. The first prediction is that due to the ram pressure interaction of the accreting gas with the magnetic islands, the correlation of $\overline{Q}/L_{\rm bol}$ and $\alpha_{\rm EUV}$ should be stronger than the correlation between $\overline{Q}$ and $\alpha_{\rm EUV}$. This was verified by a partial correlation analysis that indicated that the correlation of $\overline{Q}/L_{\rm bol}$ with $\alpha_{\rm EUV}$ is statistically significant and the correlation of $\overline{Q}$ with $\alpha_{\rm EUV}$ is spurious.

The second piece of evidence supporting magnetically arrested accretion that was found in Punsly (2015b) is a verification of the specific relationship between the jet power and the EUV suppression that arises from the basic model of magnetically arrested accretion. The derivation will not be repeated here, but the introduction of some notation is required to explain the exact result that was demonstrated. If the model is representative of the physical circumstance depicted in Figure 1 then the filling fraction of the inner accretion disk with magnetic islands, f, is related to the deficit of EUV luminosity, where the EUV luminosity deficit is evaluated relative to the luminosity of the EUV continuum of RQQs. In order to compare the EUV deficit from object to object, the EUV spectral luminosity was normalized in Punsly (2015b) to the spectral luminosity at the approximate peak of the SED,

$$\text{Normalized EUV Spectral Luminosity} \equiv \frac{L_\nu(\lambda = 700\ \text{Å})}{L_\nu(\lambda = 1100\ \text{Å})}, \tag{1}$$

where $L_\nu(\lambda = 700\ \text{Å})$ is the EUV continuum spectral luminosity and $L_\nu(\lambda = 1100\ \text{Å})$ is the spectral luminosity at the approximate peak of the SED. Defining the EUV deficit of RLQs relative to RQQs requires defining a fiducial normalized EUV spectral luminosity for RQQs from composite spectra (Punsly 2015b)

$$\text{Fiducial Normalized EUV Spectral Luminosity} \equiv \frac{L_\nu(\lambda = 700\ \text{Å})}{L_\nu(\lambda = 1100\ \text{Å})}\Big|_{\rm RQQ}, \tag{2}$$

where $L_\nu(\lambda = 700\ \text{Å})$ is the EUV continuum spectral luminosity of the RQQ composite spectrum and $L_\nu(\lambda = 1100\ \text{Å})$ is the spectral luminosity at the approximate peak of the SED in the RQQ composite spectrum. The normalized EUV deficit is approximately equal to the magnetic flux fill fraction, f, of the inner disk (equivalently the fractional volume of EUV-emitting gas that is displaced by magnetic flux tubes) in each individual RLQ

$$\text{EUV Deficit} \equiv \left[1 - \left[\frac{L_\nu(\lambda = 700\ \text{Å})}{L_\nu(\lambda = 1100\ \text{Å})}\right]\left[\frac{L_\nu(\lambda = 1100\ \text{Å})}{L_\nu(\lambda = 700\ \text{Å})}\right]\Big|_{\rm RQQ}\right] \approx f. \tag{3}$$

Since jet power scales with the square of the poloidal magnetic flux contained within the jet base, the scaling that is predicted by the basic model of magnetically arrested accretion was shown by Punsly (2015b) to be of the form

$$\overline{Q}/L_{\rm bol} \approx Af^2 \approx A\left[1 - \left[\frac{L_\nu(\lambda = 700\ \text{Å})}{L_\nu(\lambda = 1100\ \text{Å})}\right]\left[\frac{L_\nu(\lambda = 1100\ \text{Å})}{L_\nu(\lambda = 700\ \text{Å})}\right]\Big|_{\rm RQQ}\right]^2, \tag{4}$$

where A is a constant. The best fit to the RLQ data was found to be

$$\bar{Q}/L_{\rm bol} = A\left[1 - \left[\frac{L_\nu(\lambda = 700\ \text{Å})}{L_\nu(\lambda = 1100\ \text{Å})}\right] \times \left[\frac{L_\nu(\lambda = 1100\ \text{Å})}{L_\nu(\lambda = 700\ \text{Å})}\right]\bigg|_{\rm RQQ}\right]^{2.05\pm0.17}. \quad (5)$$

The uncertainty in the exponent includes uncertainty in the fiducial RQQ normalized EUV spectral luminosity in Equation (2) as well as the statistical scatter in the data. The agreement of the exponent in Equations (4) and (5) within these uncertainties provides strong evidence that the mechanism that is creating the jet and suppressing the EUV emission is in fact similar to magnetically arrested accretion in the innermost accretion disk. It is further estimated from the same analysis that f is a few percent for the RLQs with weaker jets and $\sim$50% for the RLQs with the most powerful jets (Punsly 2015b; Punsly & Marziani 2015).

4.2. Review of the EUV Deficit in the Context of Numerical Simulations

A major shortcoming of 3D numerical models of accretion onto black holes is that the magnetic field topology and poloidal flux distribution is determined by physics beyond the assumed single fluid ideal magnetohydrodynamic (MHD) approximation. This is critical because it has been shown that even small changes in the numerics near the black hole will drastically alter the poloidal magnetic flux topology and the entire dynamical scheme (Punsly 2015a, p. 149). Most prominent among these missing features is the microphysics that determines the diffusion rate of plasma onto and off of magnetic field lines and the magnetic field reconnection rate. Neither of these are well known in the exotic environment near black holes. These physical processes are critical not only for the formation of the magnetic islands, but the time evolution of the magnetic islands is determined primarily by diffusion (Igumenshchev 2008; Punsly 2015a, p. 149). Even worse, these dynamical elements occur only as a consequence of numerical diffusion in modern simulations in oversimplified ideal MHD single fluid models of the physics (Punsly 2015a, p. 149). Future development is difficult since it is not even clear theoretically what the basic principles required for an accurate physical depiction would be. Many issues that are related to these topics are active areas of investigation in solar and fusion physics (Yamada 2007; Malakit et al. 2009; Threlfall et al. 2012; Baumann et al. 2013). As such it is imperative that observational results such as those presented here are needed to guide the course of numerical and theoretical work.

The observational evidence provided by this study can be used to cull through possible numerical and physical scenarios in order to see which ones are viable candidates to represent the physical system in an RLQ. The following restrictions for numerical work are model independent and derived directly from the observations (Punsly 2015b). These can be used to guide us toward numerical models that replicate the physics of jet launching in RLQs. Empirically, it is determined that both the large-scale poloidal magnetic flux at the base of the jet and a mechanism that suppresses (but does not eliminate) the EUV emission from the innermost accretion flow coexist at the heart of the central engine of RLQs. This is too large of a coincidence; some of this magnetic flux must be the same element that disrupts but does not eliminate the innermost accretion flow. This implies that there is significant vertical poloidal magnetic flux in the inner accretion flow of RLQs. If a numerical effort cannot reproduce this circumstance, then perhaps the numerical approximation to the relevant physical processes requires further development. Observations are now mature enough to lead the numerical work.

Summarizing the status of the numerical work, it is noted that the magnetically arrested accretion discussed above in the introduction to this section is qualitatively similar to the 3D numerical simulations explored in Igumenshchev (2008) and Punsly et al. (2009). They produce a fill fraction, f, in the innermost accretion flow that is consistent with the range described below Equation (5). They also provide most of the gross features of time evolution required to support the jets and suppress the EUV emission in the innermost accretion flow (Punsly 2015b). By contrast, the simulations in McKinney et al. (2012), Tchekhovskoy et al. (2011), and Tchekhovskoy & McKinney (2012) that are heavily seeded with large-scale magnetic flux are devoid of magnetic islands close to the event horizon. This is evidenced by the claim in McKinney et al. (2012) that no significant Poynting flux emerges from this region as well as the online videos of their simulations. The videos show the innermost significant, modest, magnetic island concentrations are located at $r > 10R_g$ and they are extremely transient. In McKinney et al. (2012), Tchekhovskoy et al. (2011), and Tchekhovskoy & McKinney (2012) the fill fraction, $f \approx 0$ in the innermost accretion flow. This is basically a zone of avoidance for vertical poloidal magnetic flux in these simulations. Instead of penetrating the thickness of the equatorial accretion flow vertically, the poloidal field spreads out above and below the accretion disk in radial fans. Thus, these simulations are not consistent with the observations of RLQs. These radial fans compress or "choke" the flow. The "magnetically choked accretion flows" of McKinney et al. (2012) heat the innermost accretion flow compressively as part of the magnetic choking process and likely increase radiation from this region. This is verified by the recent results from this family of simulations (Avara et al. 2015). The inner accretion flow luminosity is claimed to increase significantly over a standard optically thick, geometrically thin accretion disk, the opposite of what is observed in RLQs.

4.3. The EUV Deficit and Jet Formation across All Scales

It is tempting to put these results into a broader context. It is possible that all black-hole-related jet phenomena are a consequence of vertical magnetic flux impeding the inner accretion flow. In particular, for Galactic black hole binaries (GBH) jet-type emission occurs only when the soft X-ray emission (the putative thermal emission from the accretion disk) is suppressed (Klein-Wolt et al. 2002; Fender et al. 2004; Russell et al. 2011). However, the "coronal" X-ray power law emission is not suppressed and can be very strong (Fuchs et al. 2003; Punsly & Rodriguez 2013).

There have also been claims that dips in the coronal X-ray flux (the X-ray power law) are coordinated with superluminal ejections in the Seyfert galaxy 3C 120 (Marscher et al. 2002; Chatterjee et al. 2009; Lohfink et al. 2013). If one were to make an analogy between the GBHs and 3C 120, the superluminal ejections in 3C 120 would have to be the equivalent of the discrete superluminal ejections in GBHs. However, superluminal discrete ejections in GBHs are characterized by very strong coronal emission in the last hours just before ejection which reach near historic maxima that can exceed 50% of the Eddington luminosity (Punsly & Rodriguez 2013). During the ejection, the X-ray luminosity becomes highly variable with an average value similar to that just before the ejection (Punsly & Rodriguez 2013). Thus, the claim of coronal X-ray power law luminosity dips in 3C 120 during superluminal ejections refers to a different phenomenon.

The corona X-ray power law emission during superluminal ejections in 3C 120 likely emerges from close to the black hole. However, there is no direct evidence that the emission from the innermost optically thick accretion flow is suppressed during superluminal ejections. The EUV emission from the high frequency tail of the optically thick thermal emission is not monitored. As noted above, in GBHs, the X-ray power law luminosity is not correlated with the optically thick thermal luminosity. Thus, there is no precedent that justifies the assumption that a dip in the X-ray power law equates to a dip in the optically thick thermal emission from the inner accretion disk in 3C 120. Thus, the physical state of the inner optically thick accretion disk during superluminal ejections is unknown. There is a claim of indirect evidence of inner disk movement outward during superluminal ejections based on Fe Kα line width arguments derived from three X-ray observations (Lohfink et al. 2013). However, the interpretation of the X-ray data in the "high state" observed with *XMM* and the inner disk location claimed by Lohfink et al. (2013) disagrees with the seminal studies of those data (Ballantyne et al. 2004; Ogle et al. 2005). The original studies of the *XMM* "high state" indicated that the Fe Kα line was produced in cold plasma at $>75R_g$ from the central black hole. This is very far from the innermost stable circular orbit (ISCO) where the cold plasma should reside if there were evidence of "a complete disk extending down to the ISCO during the *XMM-Newton* observation" as claimed by Lohfink et al. (2013, p. 83).

The claim of evidence of an interaction of the jet with the corona during superluminal ejections in 3C 120 is not well understood, primarily because the corona is not a well understood region. There is strong evidence that the corona might be an outflowing wind in Seyfert galaxies (Kharb et al. 2015; Liu et al. 2015). Does the corona envelop the disk like a stellar corona, or is it a separate, optically thin, radiatively inefficient disk inside the accretion disk (the so-called truncated disk scenario; e.g., Lohfink et al. 2013)? The physical interpretation of the depressed coronal emission is highly dependent on the model of the corona.

In summary, both GBHs and RLQs show a suppression of the optically thick thermal emission when jetted phenomena occur. The Seyfert galaxy 3C 120 shows something similar, but it is the coronal emission that appears suppressed, which does not occur in GBHs. It would be a major advance if these three phenomena could be connected. There are many poorly understood details that would need to be studied and clarified further before we reach that point.

5. CONCLUSION AND FUTURE PROSPECTS

In this paper we studied archival data on the distant quasar, 1442+101. Evidence of a real time connection between the jet power and the suppression of EUV emission is found. The result is based on only five epochs and simultaneity was established only within a 300 day interval. These findings motivate the need for a long-term monitoring program of this source and other high redshift GPSs. The radio observations would be improved with multi-frequency observations with VLA or ATCA. Knowing the flux density at more than one frequency (perhaps 8.4, 15, and 22 GHz) would allow one to compute the luminosity of the optically thin emission and would be less prone to errors induced from slight changes in spectral slope which are problematic with a single frequency proxy. Coordinated sampling two times a year would be sufficient. Ideally, the source should be monitored with the same optical and radio instruments to minimize uncertainties in this difficult measurement. The VLA "gold sample" implemented here improves the situation, but there are still multiple optical telescopes involved.

We would like to thank Tracy Clarke for supplying the VLA data from 2011 September 30. We would also like to thank Patrick Ogle and Robert Antonucci for their valuable analysis of the 3C 120 X-ray data. B.P. notes that this research was supported by ICRANet.

REFERENCES

Avara, M., McKinney, J., & Reynolds, C. 2015, arXiv:1508.05323
Baldwin, J. A., Robinson, L. B., Wampler, E. J., et al. 1974, ApJ, 104, 513
Ballantyne, D. R., Fabian, A. C., & Iwasawa, K. 2004, MNRAS, 354, 839
Barthel, P. D., Tytler, D. R., & Thompson, T. 1990, A&AS, 82, 339
Baumann, G., Galsgaard, K., & Norlund, A. 2013, SoPh, 284, 467
Blandford, R., & Znajek, R. 1977, MNRAS, 179, 433
Blandford, R. D., & Payne, D. 1982, MNRAS, 199, 883
Chatterjee, R., Marscher, A. P., Jorstad, S. G., et al. 2009, ApJ, 704, 1689
Corbin, M. 1991, ApJ, 375, 503
Dallacasa, D., Fanti, C., Fanti, R., Schilizzi, R., & Spencer, R. 1995, A&A, 295, 27
Davis, S., & Laor, A. 2011, ApJ, 728, 98
deVries, W., Becker, R., & White, R. 2006, AJ, 131, 666
Fender, R., Belloni, T., & Gallo, E. 2004, MNRAS, 355, 1105
Fuchs, Y., Rodriguez, J., Mirabel, I. F., et al. 2003, A&A, 409, L35
Grier, C., Peterson, B. M., Pogge, R. W., et al. 2012, ApJ, 755, 60
Haba, Y., Kunieda, H., Misaki, K., et al. 2003, ApJ, 599, 949
Igumenshchev, I. V. 2008, ApJ, 677, 317
Kharb, P., Das, M., Paragi, Z., Subramanian, S., & Chitta, L. P. 2015, ApJ, 799, 161
Klein-Wolt, M., Fender, R. P., Pooley, G. G., et al. 2002, MNRAS, 331, 745
Kovalev, Y. Y., Nizhelsky, N. A., Kovalev, Yu. A, et al. 2004, A&AS, 139, 545
Lind, K., & Blandford, R. 1985, ApJ, 295, 358
Liu, T., Wang, J.-X., Yang, H., Zhu, F.-F., & Zhou, Y.-Z. 2015, ApJ, 783, 106
Lohfink, A. M., Reynolds, C. S., Jorstad, S. G., et al. 2013, ApJ, 772, 83
Lovelace, R. V. E. 1976, Natur, 262, 649
Lyons, R., Cohen, R., Junkkarinen, V., Burbidge, & Beaver, E. 1995, AJ, 110, 1541
Lynden-Bell, D., & Rees, M. 1971, MNRAS Lett., 152, 461
Malakit, K., Cassak, P., Shav, M., & Drake, F. 2009, GeoRL, 36, L07107
Mantovani, F., Mack, K.-H., Montenegro-Montes, F. M., Rossetti, A., & Kraus, A. 2009, A&A, 502, 61
Markov, S., Nowak, M., & Wilms, J. 2005, ApJ, 635, 1203
Marscher, A., Jorstad, S., Gomez, J.-L., et al. 2002, Natur, 417, 625
Marshall, H. 1997, ApJ, 479, 222
McKinney, J., Tchekhovskoy, A., & Blandford, R. 2012, MNRAS, 423, 3083
Mingaliev, M. G., Sotnikova, Y. V., Torniainen, I., Tornikoski, M., & Udovitskiy, R. Y. 2012, A&A, 544, 25
Mirabel, I. F., Dhawan, V., Chaty, S., et al. 1998, A&A, 330, L9
Murphy, D., Browne, I. W. A., & Perley, R. 1993, MNRAS, 264, 298
O'Dea, C. 1998, PASP, 110, 493
Ogle, P. M., Davis, S. W., Antonucci, R. R. J., et al. 2005, ApJ, 618, 139
Pica, A. J., Smith, A. G., Webb, J. R., et al. 1988, AJ, 96, 4
Punsly, B. 2008, Black Hole Gravitohydromagnetics (2nd ed.; New York: Springer)

Punsly, B. 2014, ApJ, 797, 33
Punsly, B. 2015a, The Formation and Disruption of Black Hole Jets (Switzerland: Springer International Publishing)
Punsly, B. 2015b, ApJ, 806, 47
Punsly, B., Igumenshchev, I. V., & Hirose, S. 2009, ApJ, 704, 1065
Punsly, B., & Marziani 2015, MNRAS Lett., 453, 16
Punsly, B., & Rodriguez, J. 2013, ApJ, 764, 173
Pushkarev, A., & Kovalev, Y. 2012, A&A, 544, 34
Russell, D. M., Miller-Jones, J. C. A., Maccarone, T. J., et al. 2011, ApJ, 739, 19
Shakura, N., & Sunyaev, R. 1973, A&A, 24, 337
Shimmins, A., & Bolton, J. 1981, AuJPh, 34, 471
Smith, A., Nair, A., Leacock, R., & Clements, S. 1993, AJ, 105, 437
Stanghellini, C., Dallacasa, D., O'Dea, C. P., et al. 2001, A&A, 377, 377
Stanghellini, C., O'Dea, C. P., Baum, S. A., et al. 1997, A&A, 325, 943
Stanghellini, C., O'Dea, C. P., Dallacasa, D., et al. 1998, A&AS, 131, 303
Steppe, H., Jeyakumar, S., Saikia, D. J., & Salter, C. J. 1995, A&AS, 113, 409
Tchekhovskoy, A., & McKinney, J. 2012, MNRAS Lett., 423, 55
Tchekhovskoy, A., Narayan, R., & McKinney, J. 2011, MNRAS Lett., 418, 79
Telfer, R., Zheng, W., Kriss, G., & Davidsen, A. 2002, ApJ, 565, 773
Threlfall, J., Parnell, C. E., De Moortel, I., McClements, K. G., & Arber, T. D. 2012, A&A, 544, 24
Tingay, S. J., Jauncey, D. L., King, E. A., et al. 2003, PASJ, 55, 351
van Breugel, W., Miley, G., & Heckman, T. 1984, AJ, 89, 5
Willott, C., Rawlings, S., Blundell, K., & Lacy, M. 1999, MNRAS, 309, 1017
Yamada, M. 2007, PhPl, 14, 058102
Zhu, Y., Davis, S. W., Narayan, R., et al. 2012, MNRAS, 424, 2504